Electronic Supplementary Material (ESI) for Nanoscale.

Supporting Information

Symmetry breaking on monolayers of achiral theophylline: formation of unichiral stripes on Au(111)

Marco Pividori, Carlo Dri, Maria Elena Orselli, Federico Berti, Maria Peressi, and Giovanni Comelli*

1. Morphology of the molecular layer

As mentioned in the main paper, the ordered molecular phases always coexist with a disordered phase. A representative image of this coexistence is shown in Figure S1.

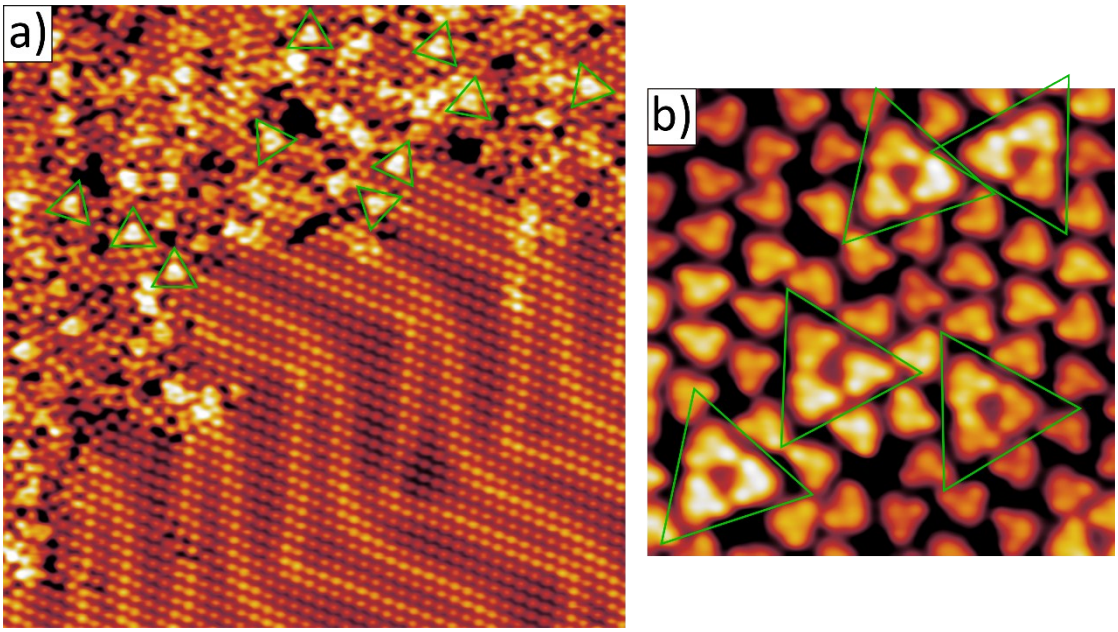

Figure S1. *Experimental STM images of a theophylline layer showing (a) the coexistence of the ordered structures with a disordered phase, where a trimer of molecules is found as a recurring motif (some of its instances are highlighted with a green marker). (b) Close-up of the disordered phase, highlighting the morphology of the trimers.*

Within the disordered phase, a characteristic motif can be identified, composed of three theophylline molecules arranged in a triangular fashion. Close inspection of these motifs (see Figure S1b) reveals that the arrangement of the molecules within the trimers is by no means regular: while the overall triangular structure is preserved, the single molecules can be attached in various conformations to each other.

2. Structure I

Figure S2 shows some additional details on the construction of the simulation cell for structure I. The blue parallelograms represent a possible choice for the periodical unit cell of the molecular layer, extracted from experiments. The experimental unit cell contains two molecules, and its sides measure 10.0 Å and 16.6 Å with an angle between the basis vectors of 53.4°.

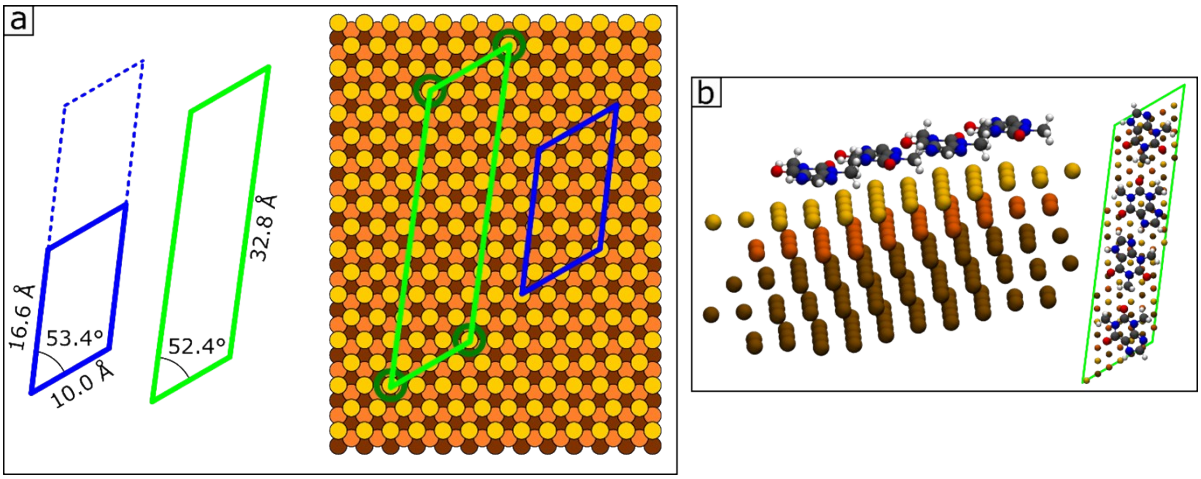

Figure S2. *(a) Comparison between the periodical unit cell observed from experiments (blue) and the simulation cell used in the calculations (green). (b) Perspective and top view of the ball and stick model of the simulation cell.*

In order to match the periodicity of the molecular layer with the one of the gold substrate, a different unit cell was used for the simulations, shown in green in Figure S2. The simulation cell (Figure S2b) contains four theophylline molecules and is very similar to the (1×2) supercell of the experimental one (dotted blue parallelogram in Figure S2), with sides of 9.99 Å and 32.8 Å and angle of 52.4°.

In the main article, we provide evidence of weak interactions between the molecular layer and the gold substrate; in the following, we describe the charge rearrangement due to the physisorption and the differences in the electronic properties.

Figure S3 shows the charge rearrangement upon adsorption of the molecular layer. Here, the charge density difference is calculated with respect to the entire molecular layer, and not with respect to the isolated molecules (as in Figure 2 of the main paper). This approach selectively reveals only the interactions between the surface and the molecular layer, while inter-layer interactions are not accounted.

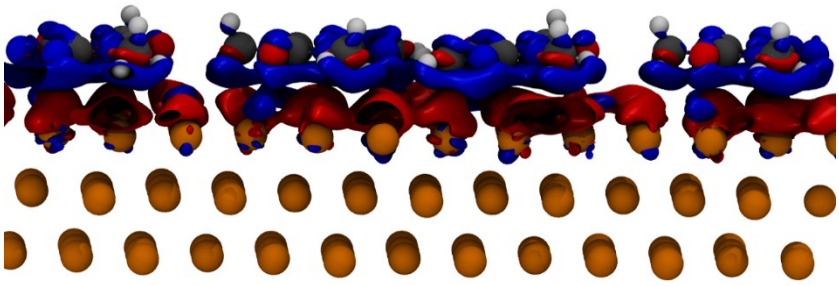

Figure S3. *Charge rearrangement with respect to the isolated constituents (gold slab and molecular layer), corresponding to isosurfaces of* $\pm 0.4e/nm^3$*. Blue/red indicate depletion/excess of electron density.*

As already stated in the main article, the charge rearrangement is uniformly distributed on the surface and does not show any directionality.

Figure S4 compares the projected density of states (PDOS) of the adsorbed structure (red) and the freestanding molecular layer (blue). The energy scales for the two systems have been aligned based on the HOMO peak of theophylline in the two cases. The first panel (Figure S4a) shows the density of states of the layer, obtained by summing the PDOS of all the atoms of theophylline molecules. The following panels (Figure S4b-i) shows the PDOS for each atom contributing to the HOMO/LUMO states. The relative intensity and the position of the peaks are almost unchanged upon adsorption, with some broadening due to the interaction with the substrate. Aligning the main PDOS peaks, there is a shift of about -0.3 eV in the Fermi level that can be associated to the charge rearrangement at the interface molecular layer/substrate. While the

freestanding layer has a null density in the HOMO-LUMO gap, the adsorbed system has some non-zero contributions that allow to obtain STM images in the low bias regime (inset of Figure S4a).

Analyzing the PDOS it is possible to understand the behavior of the STM images in the low and high bias regimes. The experimental low bias regime (Figure 1b, 4a, 7a in the main paper) correspond to energy levels within the HOMO-LUMO gap. Simulated and experimental STM images in this energy interval do not depend significantly on the applied voltage; the bias chosen for the simulations in this regime was then fixed at +1.0V, in order to guarantee a minimum number of states in the Integrated Local DOS (ILDOS) and reduce the chance of incurring in computational artifacts in the simulated STM image. The high bias regime corresponds to energies above (below) the theoretical LUMO (HOMO). Several simulations at different bias voltages above (below) the latter energy levels were performed and the main features observed in the experiment did not change significantly, supporting the hypothesis that the features observed in this regime depend essentially on the density of states at the HOMO and the LUMO. In the high bias regime, we therefore chose to simulate the images at the bias closest to the experimental value and yielding the best agreement.

The PDOS can also be used to qualitatively interpret the behavior of the STM images in the high bias regime. For positive bias, the lack of electronic states in the region between the oxygen atoms and the methyl groups is visible in the projection of the LUMO on the oxygen (Figure S4i). For negative bias, instead, the darker region corresponds to the region between the other oxygen atom and the pyrenic ring. In this case, however, we cannot identify a clear match with the PDOS of a single atom, even though there is a reduction in the electronic density of the HOMO for the atoms near that region (Figure S4d, f).

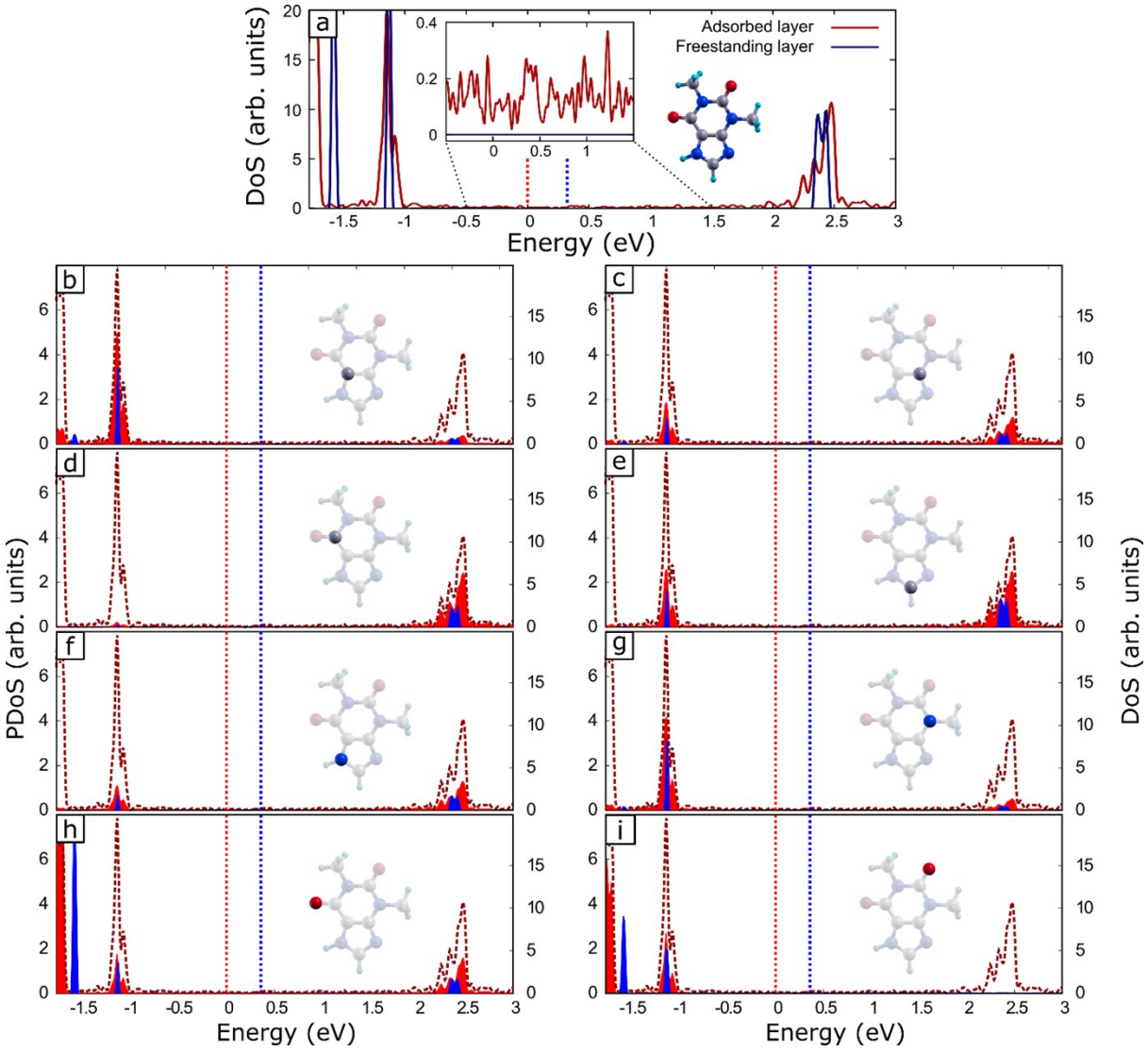

Figure S4. *Electronic structure for adsorbed (red) and freestanding (blue) molecular layer. (a) Total Density of States (DoS) for the two systems, obtained by summing the projected DoS (PDoS) over all the atoms belonging to theophylline. Inset: zoom of the DoS in the HOMO-LUMO gap region. (b) - (i) Filled curves (red/blue for adsorbed/freestanding layer) shows the PDoS related to the highlighted atoms; the total DoS of the adsorbed system (red dashed curve) is reported for comparison. In all the plots the zero of the energy scale is set to the Fermi level of the adsorbed system (red dotted vertical lines), whereas blue vertical lines shows the relative Fermi energy of the freestanding layer.*

A final remark concerning structure I is related to the inter-molecular interactions within the adsorbed layer and, in particular, the definition of the interaction energies and the evaluation of the dispersive interactions. In the main article, we defined the interaction energies using freestanding values, both for the molecular layer (E_{inter}) and for the isolated molecules ($E_{ads}^{molecule}$), in order to compare our values with the existing literature on related systems. Conversely, an alternative definition for the interaction energies is:

$$E_{cohesive} = -\frac{E\left(layer/Au^{(1)}\right) - N(molecule)E\left(molecule/Au^{(2)}\right) + E(Au^{*})}{N(molecule)}$$

In this definition, the energies of the adsorbed layer and of the single adsorbed molecule are compared. In order to account for the different number of gold atoms in the two simulations ($Au^{(1)}$ for the layer and $Au^{(2)}$ for the isolated adsorbed molecule), a metal slab energy term is added to the equation ($E(Au^{*})$). Using this expression for structure I gives a cohesive energy of 0.70 eV, to be compared with the interaction energy value provided in the main article (0.65 eV). Since the difference is only slightly larger than the computational

accuracy, we decided to stick with the definition given in the main text. Moreover, since the description of the gold slab changes between the different analyzed structures, systematic errors may arise and the freestanding expression is therefore preferable when comparing results from different structures.

In order to evaluate the dispersion interactions that connect the double rows of molecules internally bonded by H-bonds, two sets of simulations were performed, using a theophylline dimer, and double-rows of molecules, respectively. For simplicity, both tests were performed in a freestanding setup.

In the first case, an isolated dimer of theophylline was simulated, with the molecules facing through the $CH_3 \cdots O$ region. The total energy of the system was compared with the energy of the two isolated molecules and was studied as a function of their reciprocal distance. The resulting interaction energy of the system was found to be at most 0.02 eV, comparable with the computational errors.

To further check this interaction, another simulation was performed using isolated double rows of molecules. In this case, the molecules were facing through the H-bond network and the dispersive interaction energy was evaluated subtracting the energy of the isolated double-row to the energy of the overall system.

$$E_{dispersive} = -\frac{E(layer) - E(doublerow)}{2}$$

With this definition, the estimated interaction energy in the dispersive region amounts to 0.08 eV, remarkably small with respect to the previously discussed inter-molecular hydrogen bonding.

3. Structure II

Concerning structure II, building the trial configuration starting from the low bias experimental STM images was more complex than for the previous structure. In particular, as can be seen in Figure S5a or in the main article, the “L-shape” that allowed a clear classification between the different chirality is not as distinct as in structure I, thereby preventing a reliable assignment of molecular chirality. To overcome this obstacle, an internal symmetry within the molecular lattice was exploited.

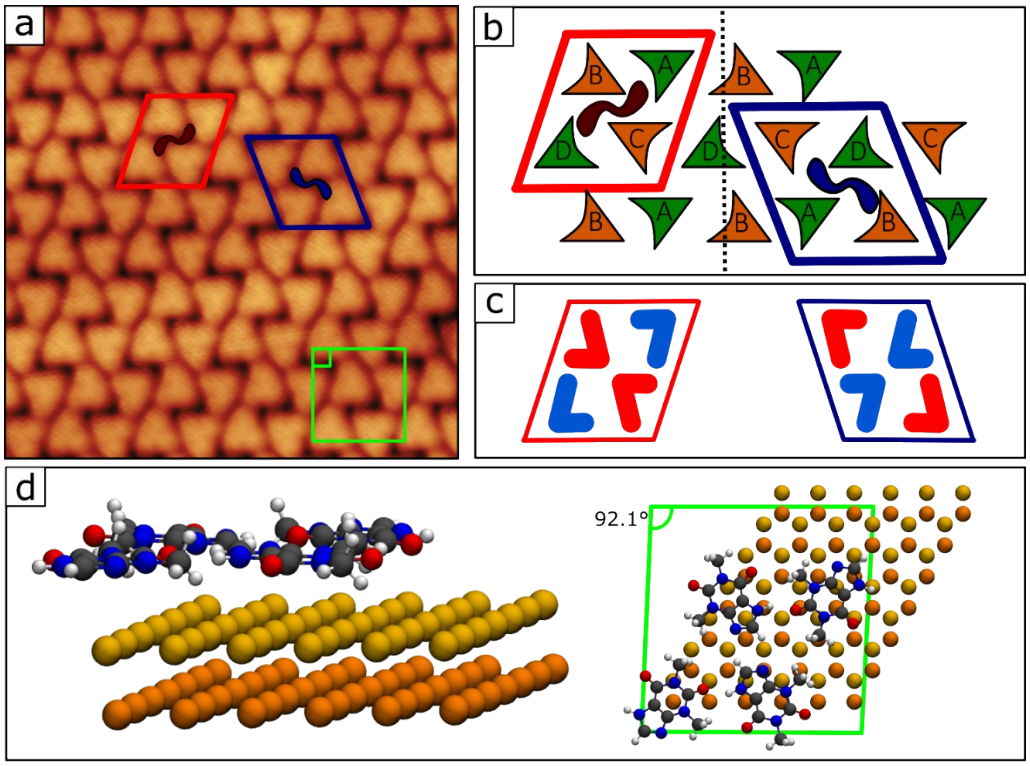

Figure S5. *Internal symmetry observed in structure II. (a) Experimental STM image of structure II at low bias. Red and blue parallelograms represent two different units with internal bases that can be used to tile the surface, while the green rectangle shows the unit cell of the molecular layer. (b) Tentative model for structure II after imposing both periodicity and internal symmetry; the molecules are labelled according to the periodicity of the molecular lattice and the different colors refer to different enantiomers. The two internal bases are related by reflection symmetry (black dotted vertical line). (c) Final model for the internal bases of structure II, using the same L-shapes from structure I for clarity. (d) Perspective and top view for the ball and stick model of the simulation cell for structure II (the green line highlights the borders of the simulation cell).*

The four molecules of the periodic cell can be grouped in two distinct units with internal bases, drawn in red and dark blue in Figure S5. These two units can be equivalently used as building blocks to create the overall molecular layer and they appear to be related by a reflection symmetry (Figure S5b, c). The observation of this internal symmetry simplifies the construction of the periodic cell: by imposing both the internal symmetry and the periodicity of the molecular lattice, it is possible to obtain specific constraints for the orientation of the molecules within the cell. In particular, if the molecules are labelled as in Figure S5b, the following relations are valid:

$A = C^*$

$B = D^*$

where the star sign indicates a reflection operation with respect to the axis drawn in the figure. With these relations, the system is racemic by construction, since the reflection operation switches chirality. The number of independent molecules in the unit cell is also reduced to two.

Another issue concerning the simulation cell of structure II is related to the matching with the substrate. Figure S6 shows the periodic cell for the molecular layer obtained from the experimental image (blue parallelogram). Since it is not possible in STM to image simultaneously the surface atoms and the molecular layer, the registry and commensurability between the two cannot be determined experimentally and the real periodic cell of the entire adsorbed system must be inferred from the geometrical properties of the molecular layer. The green parallelogram represents our choice of simulation cell, which is the smallest cell that has a perfect match with the gold substrate and carries the best similarity with the experimental cell. A periodic cell that grants both a match with the substrate and the molecular layer (i.e. blue dotted parallelogram) is

not computationally viable. As can be observed from Figure S6, the experimental cell is not exactly equivalent to the cell we used, since there is a deformation of about 2.1°. The simulated STM images presented in the main article have been slightly skewed, in order to partially correct for this error.

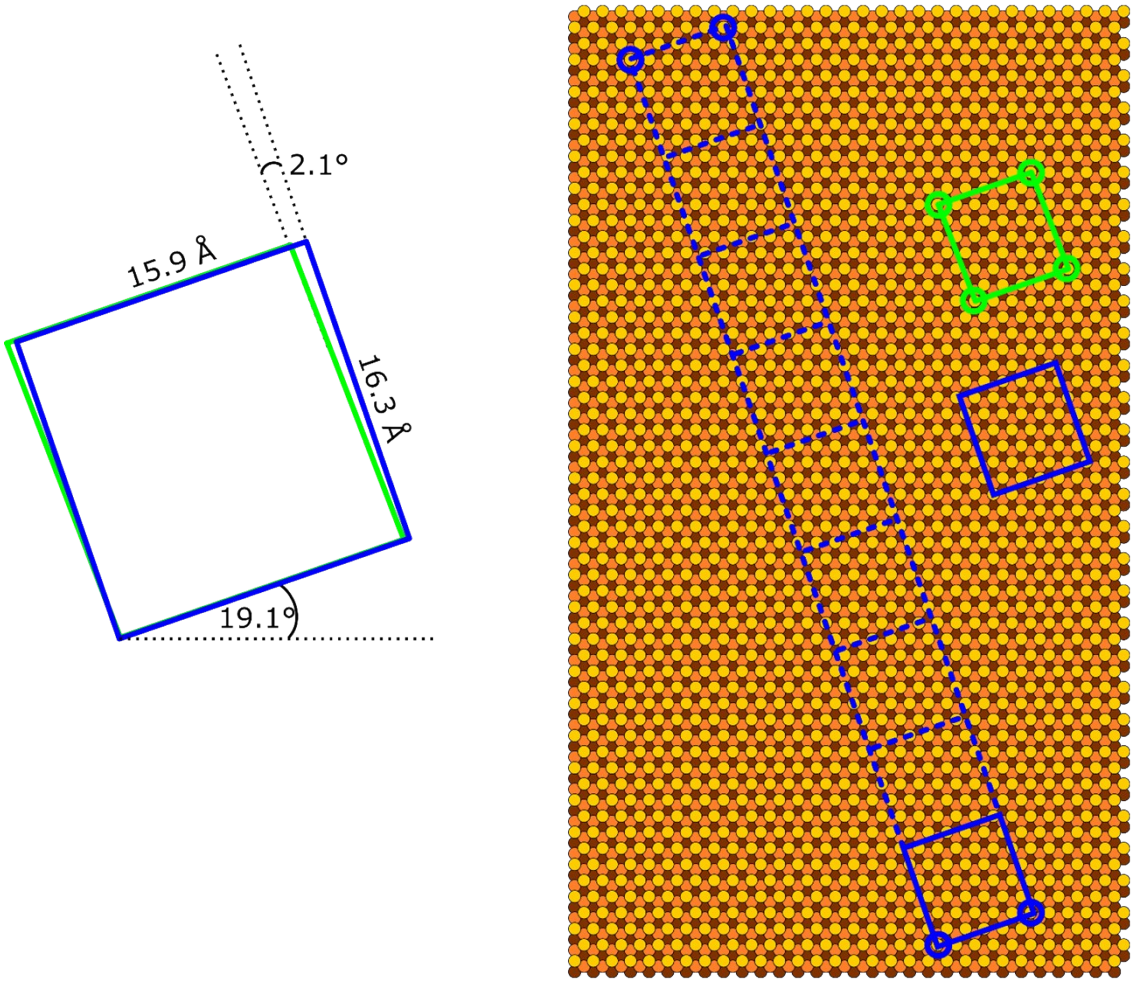

Figure S6. *Matching of the simulation cell of structure II with the gold substrate. The blue parallelogram represents the experimental cell for the molecular lattice, obtained from the periodicity of the experimental STM images. The green parallelogram is the smallest cell that has a perfect match with the substrate and carries the best similarity with the experimental cell. On the right, a possible cell for the overall system is drawn in dotted blue.*

4. Domain boundaries

As already discussed in the main paper, it was not possible to obtain a fully reliable model of the initial configuration for the domain boundary from the STM image only, especially concerning the identification of the molecular chirality and orientation.

The four configurations that best match the low bias STM images are shown in Figure S7. The criterion used to build these configurations is the triangular shape of the molecules, which imposes a constraint on their orientation. Since the chirality could not be clearly recognized in the STM images (the “L-shape” is not as clear as in structure I), the different configurations were obtained by looking at the long sides of the triangles and considering all the possible permutations of the chirality. Two of the trial configurations (unichiral I and unichiral II) present a local excess of chirality in the domain boundary. The other two configurations are racemic and actually equivalent, since they transform into each other by performing a 180° rotation in the molecular plane (the boundary is symmetric upon this operation).

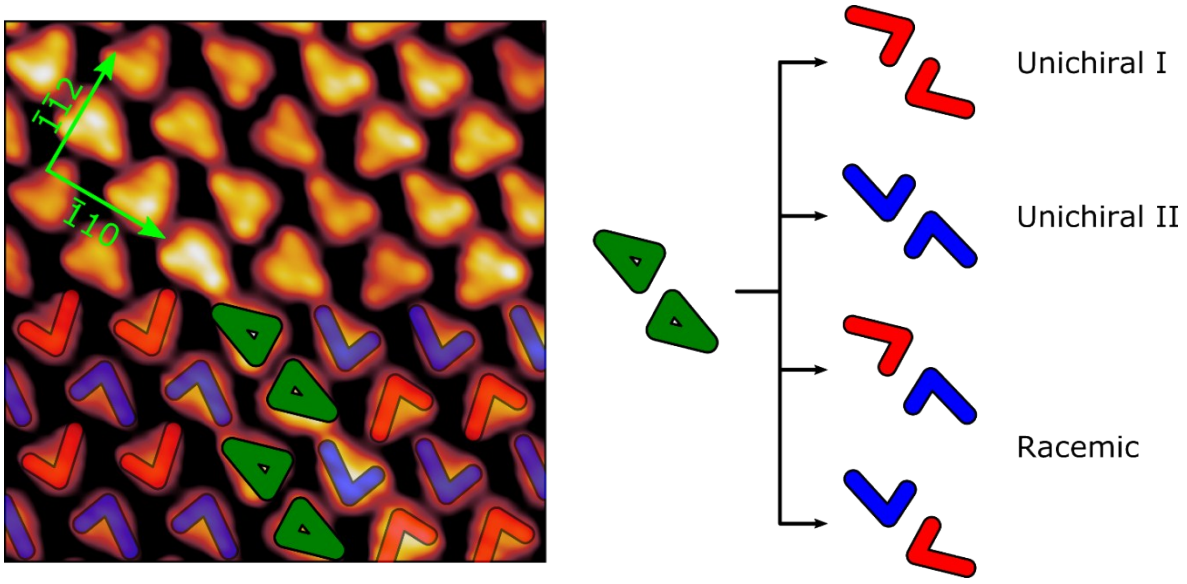

Figure S7. *Possible models for the domain boundary structure. Green isosceles triangles are superimposed to the STM image, together with their possible attribution to blue and red Ls, highlighting the four possible trial configurations. The two racemic configurations are equivalent through a 180° rotation.*

The stability of the three inequivalent systems was calculated using the interaction energy of the freestanding system, but the difference between the three values was within the computational accuracy, thus preventing an unambiguous identification of the best model from energetic criteria. Therefore, albeit less quantitatively, in order to single out the most appropriate model we resorted to the comparison between the appearance of the simulated and experimental images, as discussed in the main paper.

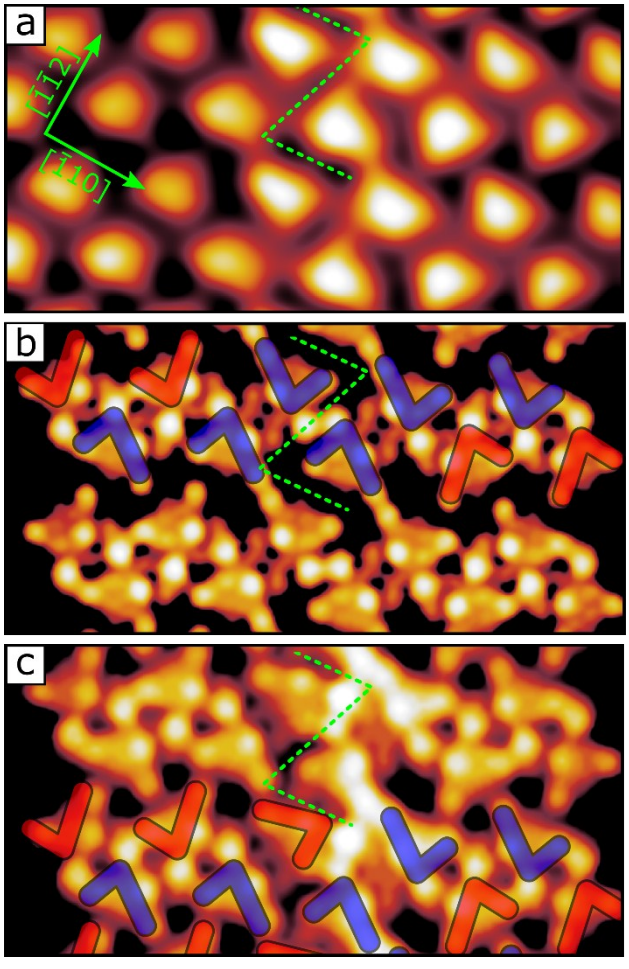

Figure S8. *(a) experimental STM image of a descending domain boundary. Simulated STM images of models of the boundary constituted by (b) Si (blue) enantiomers and (c) alternated Re (red) and Si enantiomers. The green dashed lines guide the eye to follow the characteristic dark zig-zag pattern of the high voltage image of the boundary. Image parameters: (a)* $V_s = 3.45\ V$, $I_t = 0.01\ nA$; *(b,c)* $V_s = 3.40\ V$, $ILDoS = 1.12 \times 10^{-4} e/nm^3$; *all images* $5.55 \times 2.78\ nm^2$.

As mentioned in the main paper, in order to validate the unichiral I model, we have also simulated the STM images for the models corresponding to the other two possible enantiomeric compositions of the *descending* boundary, i.e. unichiral II and racemic. The comparison between experiment and theory for these alternative arrangements of the boundary is shown in Figure S8. Once again, in the simulated images it is not straightforward to identify the single molecules. However, for both trial molecular arrangements (Figure S8b-c), the distinctive features of the boundary region are now very different from the experiment. In fact, the unichiral *Si* boundary (Figure S8b) now shows a bright protrusion in the long part of the *zig-zag* (green dashed line), where a dark contrast is instead observed in the measured STM image (Figure S8a). Also, in the racemic boundary (Figure S8c), asymmetric bright features appear on the *zig-zag*, that are not present in the experimental image.